Biomolecule Identification Using Superlattice AlGaN/GaN High-K MOSHEMT: A Cutting-Edge Biosensing Technique

Tulip Kumar Saha
National Institute of Technology Mizoram
Moumita Mukherjee
drmmukherjee07@gmail.com
Adamas University
Rudra Sankar Dhar
National Institute of Technology Mizoram

Research Article

Keywords: Biosensor, 2DEG, high-K dielectric, threshold voltage, sensitivity, label free detection

Posted Date: October 13th, 2023

DOI: https://doi.org/10.21203/rs.3.rs-3400370/v1

Additional Declarations: No competing interests reported.

Version of Record: A version of this preprint was published at Microsystem Technologies on August 27th, 2024. See the published version at https://doi.org/10.1007/s00542-024-05738-4.

Biomolecule Identification Using Superlattice AlGaN/GaN High-K MOSHEMT: A Cutting-Edge Biosensing Technique

Tulip Kumar Saha[1,2], Moumita Mukherjee[3, *] and Rudra Sankar Dhar[1, *]

[1]Department of Electronics and Communication Engineering, National Institute of Technology Mizoram, Aizawl 796012, India
[2]Department of Electronics and Communication Engineering, School of Engineering and Technology, Adamas University, Kolkata 700126, West Bengal, India and
[3]Department of Physics, School of Basic and Applied Science, Adamas University, Kolkata 700126, West Bengal, India

drmmukherjee07@gmail.com, rudra.ece@nitmz.ac.in

Abstract. This paper presents biomolecule identification process using a novel biosensing technique with high-K metal-oxide-semiconductor high electron mobility transistor (MOSHEMT). The authors have simulated a MOSHEMT device with high-K dielectric material to improve the sensitivity of biosensors. High-K dielectric material is utilized to examine the electrical efficacy of MOSHEMT-based biosensors. When high-K materials are used, Two-Dimensional Electron Gas (2DEG) benefits from carrier confinement and leakage current reduction. Therefore, the on-current of the device has been increased. For numerical modeling, TCAD Silvaco Atlas is used. For label-free identification of biomolecules, simulator is used to investigate and compare various performance parameters with SiO_2 MOSHEMT. Experimental evidence verifies the accuracy of the model. According to the authors' knowledge, this is the first investigation on high-K dielectric AlGaN/GaN MOSHEMT biosensors for efficient label-free biomolecule detection. AlGaN/GaN MOSHEMTs, which use a high-K material, are found to be promising for use in biosensors.

Keywords: Biosensor, 2DEG, high-K dielectric, threshold voltage, sensitivity, label free detection.

1 Introduction

Using contemporary biosensor technology, viruses, nucleic acids, proteins etc can be detected. There are numerous applications for biosensors based on field-effect transistors (FETs), such as food analysis, criminal investigation, medical diagnosis, and the study of biomolecule interactions [1].

Researchers from around the world have devoted a great deal of time and energy for the development of FET-based biosensors for recognizing various categories of biomolecules. According to research by K.H. Chen et al., 2DEG concentration changes caused by differences in surface charge are used to identify breast cancer through the c-erbB-2 antigen [7]. Choi et al. proposed a biosensor based on high-K gate dielectric DMFET in order to prevent short-channel effects (SCEs) [8]. D.S. Kim et al. exhibited a charge sensor based on MOSFET for the identification of DNA [9]. C.H. Kim et al. reported about NeCMOS for the detection of DNA sequence [10]. As demonstrated by Lee et al., the highly pathogenic Avian Influenza (AI) virus was detected using a nanogap field-effect transistor (FET) [11]. Maesoon et al. proposed nanogap-DGFETs

for the identification of AI virus [12]. Sarkar et al. reported a sensitivity comparison between impact ionization field-effect-transistor (IFET) [13] and tunnel field-effect-transistor (TFET) with conventional FET (CFET) biosensors for pH sensing.

Kenzo Maehashi et al. fabricated a biosensor based on CNT-FETs for label-free detection of IgE [15]. Kannan et al. introduced an UI-MOS based sensor for identification of charged nano-biomolecules [16]. G. Seo et al. constructed graphene-based FET biosensor to identify the SARS-CoV-2 virus [17]. Pratap et al. developed a GAAJLT with an integrated nanogap for identification of neutral biomolecules such as Uricase, Streptavidin, Protein, ChOx, and APTES [18].

In HEMT device the consequence of band bending causes the alignment of the Fermi level. The direction perpendicular to the heterointerface has been chosen as quantized direction (z-direction). The x-direction and the y-direction are selected along the length and width of the device, respectively. Due to the high electron mobility of 2DEG, AlGaN/GaN MOSHEMTs are predicted to exhibit lower device on-resistance and faster switching speed than SiC devices. Because of the existence of 2DEG at the AlGaN/GaN heterointerface [6], AlGaN/GaN demonstrates biosensing applications. In this paper authors have made an extensive comparative analysis with the existing literature [1]. Maximum sensitivity that has been achieved so far is 0.19734 using dual cavity of 2 µm cavity length for detection of Unicase [2]. Researchers are trying hard to develop highly sensitive biosensors for accurate detection of biomolecules. The authors have made an attempt to address this issue of low sensitivity by introducing high-K dielectric in this present paper. To demonstrate the excellence of the structure proposed in this paper, a thorough comparative analysis [1] of existing studies has been performed. Different biomolecules can readily adhere to the AlGaN barrier, resulting in surface charges at the AlGaN/GaN heterointerface. For label-free detection of biomolecules, a design-optimized structure of AlGaN/GaN MOSHEMT-based biosensors has been proposed in this work. The second section contains the device design (in-silico). The simulated device in the present model is discussed in Section 3. In Section 4, we present simulated results for the detection of various biomolecules, the proposed fabrication method is described in Section 5, and in Section 6, we conclude our research.

2 Device Design (In-Silico Study)

Figure 1(a) depicts the schematic cross-section of designed biosensor based on AlGaN/GaN MOSHEMT, for which the authors have incorporated HfO_2 as a high-K dielectric material. The function of SiO_2 is also studied in order to make a comparative analysis. The structure is made up of a barrier layer of t_{AlGaN}=18 nm $Al_{0.2}Ga_{0.8}N$ on above a buffer layer of 2.0 µm GaN, both of which were produced on a Sapphire substrate. To mimimize the lattice mismatch caused by the GaN buffer and the Sapphire substrate, a 10 nm AlN spacer layer is being introduced. The authors have carried out device structure optimization in order to achieve highest level of device performance in terms of different electrical parameters such as drain current, sensitivity and threshold voltage. The barrier, buffer and spacer layer widths have been varied in between 25 nm to 15 nm, 1 µm to 3 µm and 5 nm to 25 nm respectively. In addition to this role of gate metal on electrical characteristics of the device are considered for performance optimization study. To do so, authors have considered the role of Ni/Au and Pt as Schottky gate metal in achieving optimal performance where Pt gives better performance. Aluminium is utilized in the formation of source and drain ohmic contacts. The distance between source and gate is 2.5 µm, the distance between the gate and the drain is 1 µm, and the distance between the drain and the source is 4.5 µm. Figure 1(b) demonstrates that the region beneath the gate electrode was filled with HfO_2, a nano-cavity measuring 400 to 600 nm in length and 20 nm in width was created. On top of an AlGaN barrier layer, a nano-cavity is fabricated for biomolecule detection. For optimal device efficacy, the gate should be positioned near the source [3-4].

Each of the simulations are done using Silvaco Atlas. Calibration is essential for validating the suggested model and methodologies used in TCAD simulation. Figure 2 shows output

characteristics (I_D-V_D) for simulated device with gate voltage, V_G=-4 V with L_G=1.5 µm and corresponding experimental results are shown under similar electrical operating conditions.

This has clearly established the validity of the simulated model and based on high-K biosensor, MOSHEMT structure is designed and analysed. The models used are FLDMOB model, albrct.n, cal.strain, srh model, polarization model, and conmob model. AlGaN/GaN heterointerface is assumed to have an interface charge of 8.8×10^{12} cm^{-2}.

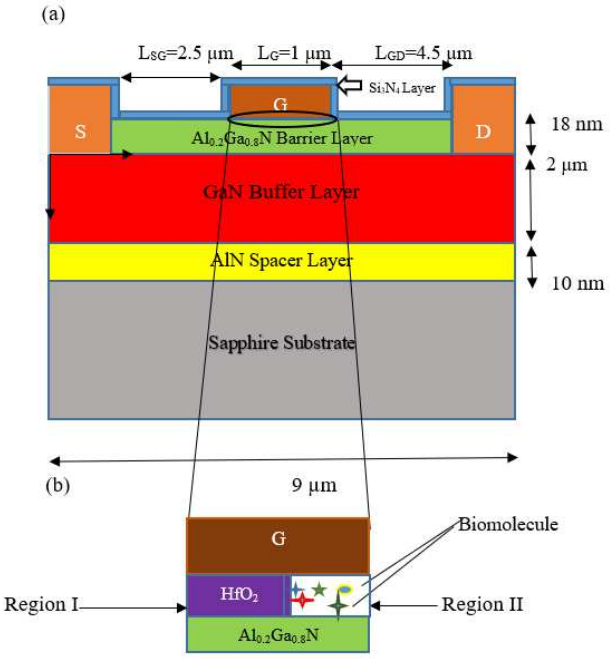

Fig. 1. Nano-cavity beneath the gate electrode of an AlGaN/GaN high-K MOSHEMT (b) Magnified image of nano-cavity under gate.

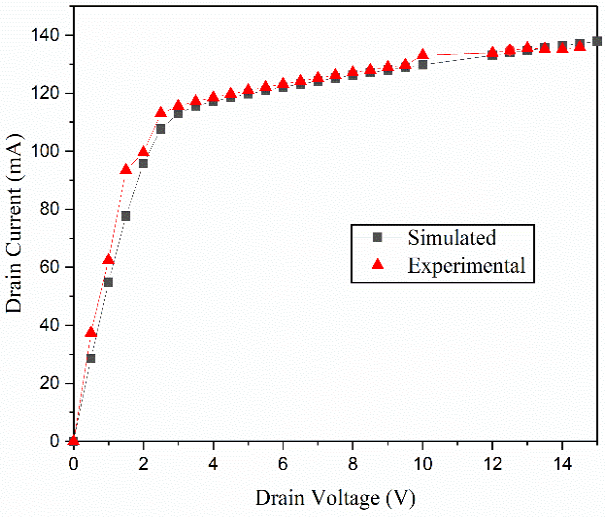

Fig. 2. I_D vs V_D with V_G=-4 V and L_G=1.5 µm, as shown in simulations and experiments [19]. Current Model

The gate-to-drain distance (L_{GD}) and oxide layer thickness (t_{ox}) are essential parameters that influence the usefulness of the device. In figure 1(b) capacitance for region-I and region-II are C_{HfO2} and C_{Bio} respectively.

$$C_{HfO2} = \frac{\varepsilon_{HfO2}}{t_{ox}} \quad (1)$$

$$C_{Bio} = \frac{\varepsilon_{Bio}}{t_{Bio}} \quad (2)$$

Where $\varepsilon_{HfO2}, \varepsilon_{Bio}$, t_{ox} and t_{Bio} are permittivity and thickness of HfO2 and biomolecule respectively. For simplicity

$$t_{ox} = t_{Bio} \quad (3)$$

The effective capacitance of region-I and II is given by

$$C_T = C_{HfO2} + C_{Bio} \quad (4)$$

Effective capacitance of MOSHEMT biosensor [20] is given by

$$\frac{1}{C_{MOSHEMT}} = \frac{1}{C_{HEMT}} + \frac{1}{C_T} \quad (5)$$

where C_{HEMT} is the capacitance of HEMT and given by

$$C_{HEMT} = \frac{\varepsilon_{AlGaN}}{t_{AlGaN}} \quad (6)$$

t_{AlGaN} and ε_{AlGaN} are the thickness and dielectric constant of AlGaN, barrier layer respectively. As dielectric constant of AlGaN, barrier layer depends on the mole fraction, x [21] and is given by

$$\varepsilon_{AlGaN} = -0.3x + 10.4 \quad (7)$$

Total capacitance of MOSHEMT biosensor is given by

$$\frac{1}{C_{MOSHEMT}} = \frac{1}{C_{HEMT}} + \frac{1}{C_{HfO2} + C_{Bio}} \quad (8)$$

The quantum well (QW) is formed at AlGaN/GaN heterointerface and charge concentration in QW is calculated [22] using triangular well approximation and considering only two subbands

$$n_s = DV_{th}[\ln(1 + e^{\frac{(E_f - E_0)}{V_{th}}}) + \ln(1 + e^{\frac{(E_f - E_1)}{V_{th}}})] \quad (9)$$

$D = 3.24 \times 10^{17}\ m^{-2}V^{-1}$ is the density of states, The energy of these subbands are given by [23]

$$E_{0,1} = \gamma_{0,1} n_s^{2/3} \quad (10)$$

$\gamma_0 = 2.26 \times 10^{-12}\ V.m^{4/3}$ and $\gamma_1 = 4 \times 10^{-12}\ V.m^{4/3}$ are the adjustable parameters [24] V_{th} is thermal voltage and equal to $\frac{kT}{q}$ where q represents the charge of an electron, T represents the operating temperature, and k is the Boltzmann constant. At the AlGaN/GaN heterointerface, a triangular quantum well is formed, and the second energy level, E_1 is considerably greater compared to the first energy level, E_0 and the Fermi level, E_f for the total operating range of the applied gate voltage, V_G and $V_{go} = V_G - V_{off}$ where V_{off} is the cutoff voltage.

$$n_s = DV_{th}[\ln(1 + e^{\frac{(E_f - E_0)}{V_{th}}})] \quad \text{as } E_1 >> E_0, E_f \quad (11)$$

$$E_f = \gamma_0 n_s^{2/3} + V_{th} \ln[e^{\frac{n_s}{DV_{th}}}] \quad (12)$$

$$V_{go} = E_f + \frac{qt_{AlGaN} n_s}{\varepsilon_{AlGaN}} \quad (13)$$

The drain current is given as,

$$I_D = \frac{q\mu W}{L} \int_{V_S}^{V_D} n_s dV \quad (14)$$

where W is the width of the channel and L is the length of the channel. V_D and V_S are the drain and source voltage respectively.

The drain current is given by [22]

$$I_D = -\frac{q\mu W}{L}\left[\frac{q}{2C_{HEMT}}(n_D{}^2 - n_S{}^2) + \frac{2}{5}\gamma_0(n_D{}^{5/3} - n_S{}^{5/3}) + V_{th}(n_D - n_S)\right] \quad (15)$$

where n_D and n_S are the charge concentration of charge carrier at drain and source terminals respectively.

3 Results and Discussions

At L_{Cavity}=500 nm, W_{Cavity}=20 nm, and V_D=5 V, various biomolecules are incorporated into the nano-cavity to produce the I_D-V_G curves shown in figure 3. The on-current, I_{ON} increases with decrease in permittivity of biomolecules.

Since sheet charge density is predominantly influenced by the polarization charge in the channel, both lattice mismatch and sheet charge density increase as the mole fraction increases. More drain current is obtained in the AlGaN/GaN HEMT due to the polarization effect than in the case when the polarization effect is ignored at a lower mole fraction, x=0.2 and t_{AlGaN}=18 nm.

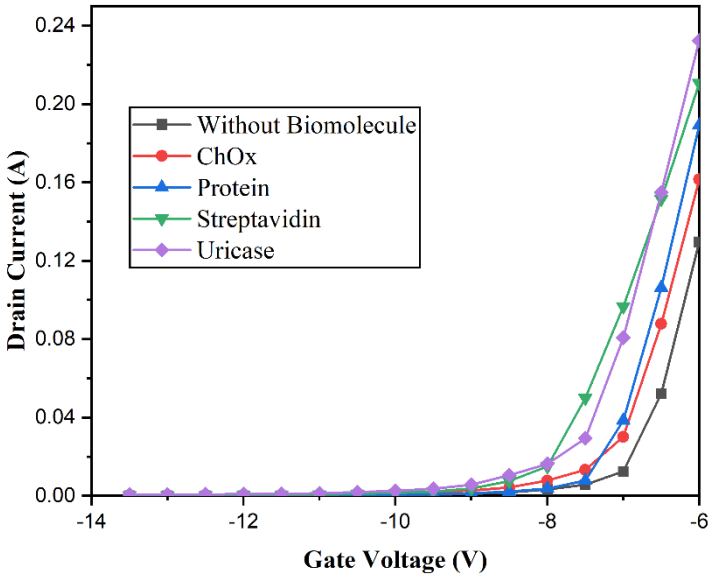

Fig.3. I_D-V_G curve for without cavity with V_D=5 V and different biomolecules using high-K MOSHEMT with t_{AlGaN}=18 nm and x=0.2.

The I_D-V_G curves in Figure 4 (a)-(e) are produced for three distinct MOSHEMT structures, including MOSHEMT-1 with t_{AlGaN}=25 nm, x=0.3, MOSHEMT-2 with t_{AlGaN}=18 nm, x=0.3, and MOSHEMT-3 with t_{AlGaN}=18 nm, x=0.2, all with HfO_2 as the dielectric. The decreasing dielectric constant of sensitive biomolecules increases the on-current, I_{ON}. The variations in drain current for the different nano-biomolecules such as Uricase, Streptavidin, Protein, and ChO_X, are shown in Figure 4 (a)–(e). While the drain current variation for ChO_X is lower 0.0105 A, 0.132 A, and 0.178 A respectively for the three different structures of HfO_2 MOSHEMT biosensors, the drain current variation for Uricase, a biomolecule with a smaller dielectric constant is larger 0.0138 A, 0.195 A, and 0.232 A respectively for the three different structures of HfO_2 MOSHEMT biosensors.

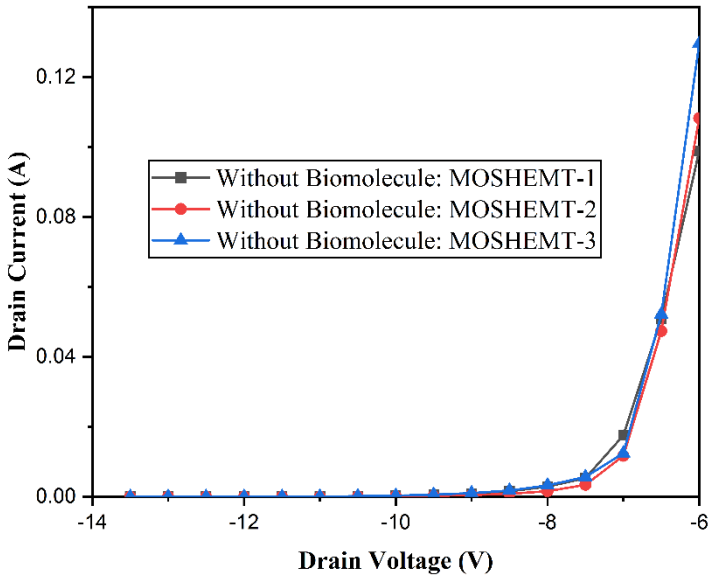
Without Biomolecule: MOSHEMT-1
Without Biomolecule: MOSHEMT-2
Without Biomolecule: MOSHEMT-3
Drain Current (A)
Drain Voltage (V)
0.00
0.04
0.08
0.12
-14
-12
-10
-8
-6

(a)

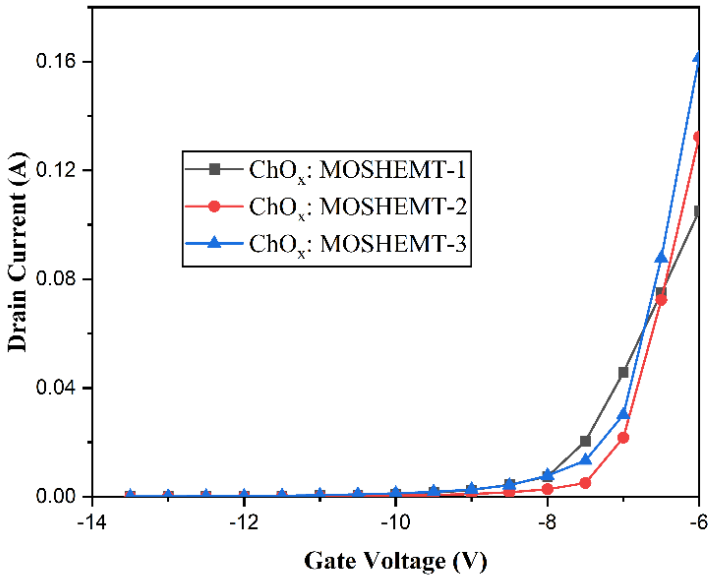
ChO$_x$: MOSHEMT-1
ChO$_x$: MOSHEMT-2
ChO$_x$: MOSHEMT-3
Drain Current (A)
Gate Voltage (V)
0.00
0.04
0.08
0.12
0.16
-14
-12
-10
-8
-6

(b)

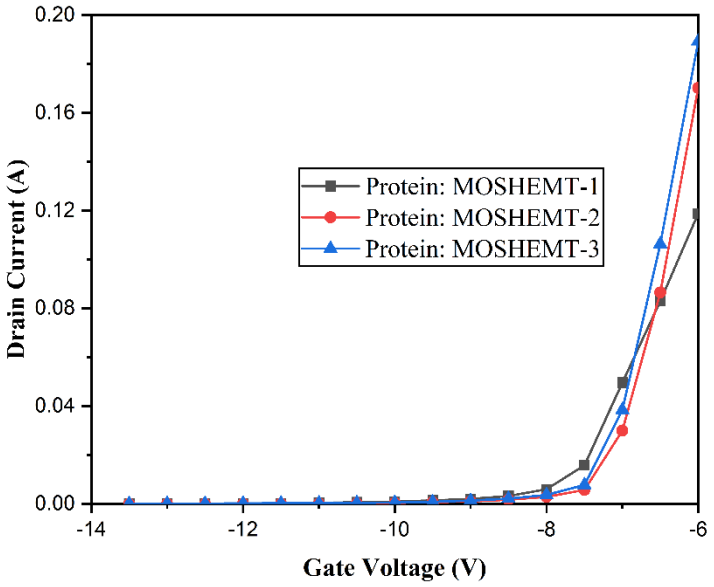
0.20
0.16
0.12
0.08
0.04
0.00
Drain Current (A)
-14
-12
-10
-8
-6
Gate Voltage (V)
Protein: MOSHEMT-1
Protein: MOSHEMT-2
Protein: MOSHEMT-3

(c)

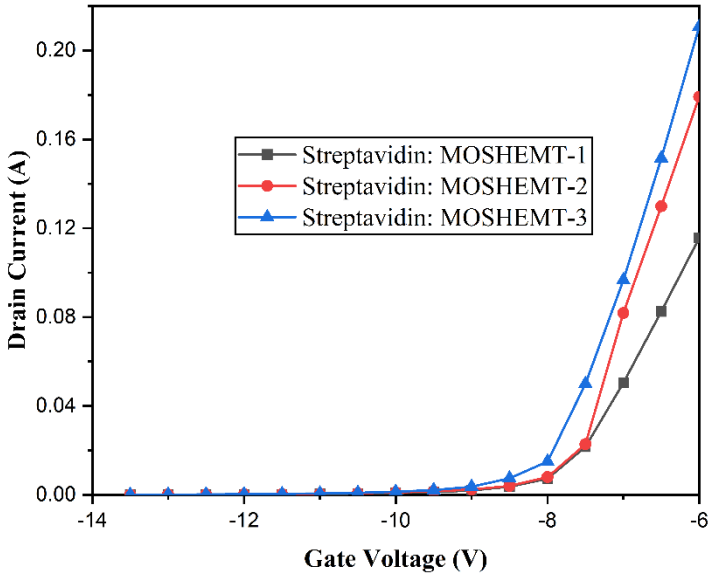
0.20
0.16
0.12
0.08
0.04
0.00
Drain Current (A)
-14
-12
-10
-8
-6
Gate Voltage (V)
Streptavidin: MOSHEMT-1
Streptavidin: MOSHEMT-2
Streptavidin: MOSHEMT-3

(d)

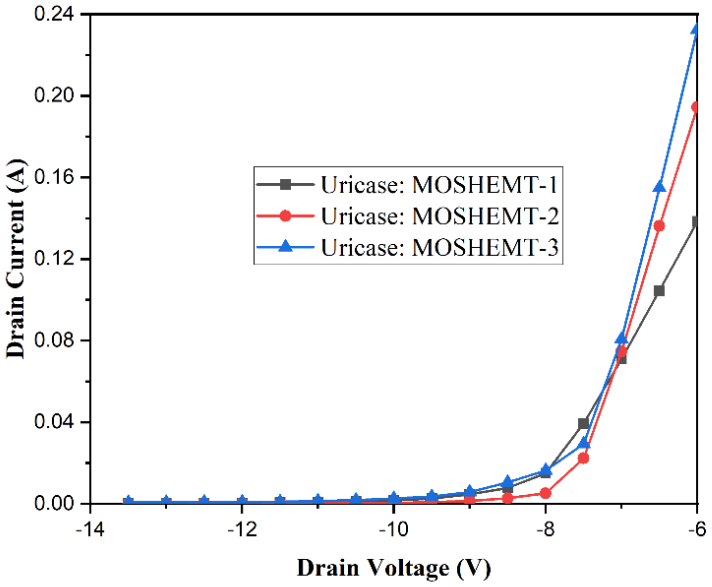

(e)

Fig.4. I_D-V_G curve for without cavity with V_D=5 V and different biomolecules using high-K MOSHEMT. Here MOSHEMT-1: t_{AlGaN}=25 nm, x=0.3, MOSHEMT-2: t_{AlGaN}=18 nm, x=0.3, MOSHEMT-3: t_{AlGaN}=18 nm, x=0.2.

Figure 5 depicts the effect of varying V_G=-4 V and tAlGaN=18 nm and x=0.2 on I_D- V_D for various biomolecules and without a cavity.

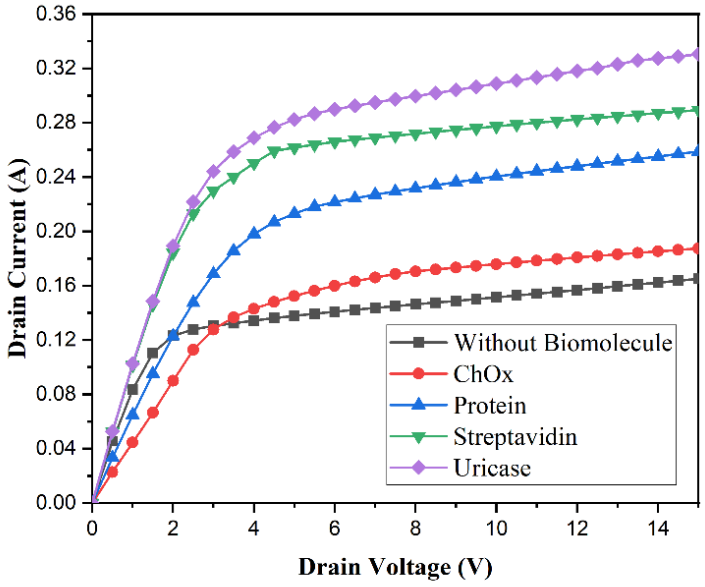

Fig.5. I_D- V_D curve for different biomolecules and without cavity with V_G= -4 V using MOSHEMT based on high-K material with t_{AlGaN}=18 nm and x=0.2.

By adding various nano-biomolecules into the nano-cavity, the I_D-V_D curves depicted in Figures 6(a)-(e) are obtained at V_G= -4 V for L_{Cavity}=500 nm and W_{Cavity}=20 nm. The 2DEG confinements at the AlGaN/GaN heterointerface increases due to the

incorporation of high-K materials. Results demonstrate that MOSHEMT-3 structures with smaller lattice mismatch have higher drain currents.

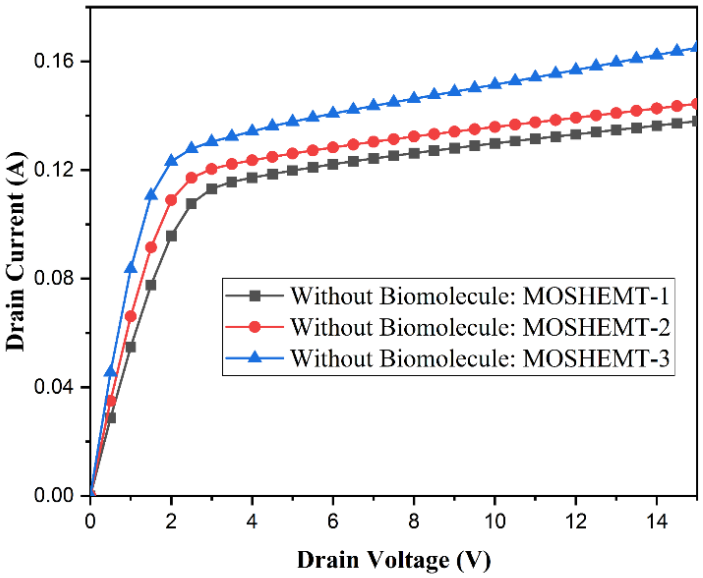

(a)

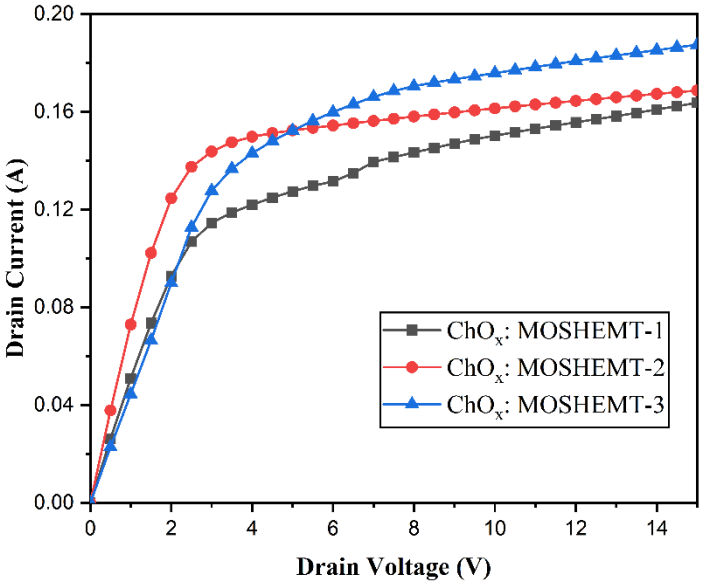

(b)

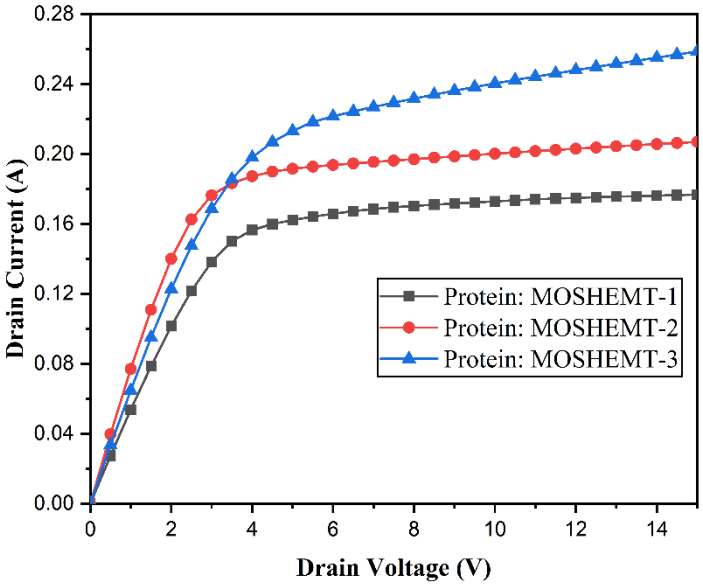
Drain Current (A)
Drain Voltage (V)
Protein: MOSHEMT-1
Protein: MOSHEMT-2
Protein: MOSHEMT-3

(c)

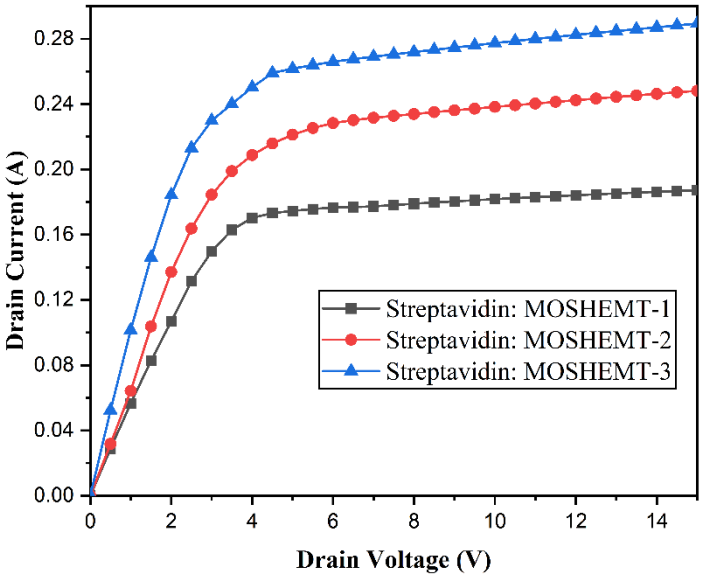
Drain Current (A)
Drain Voltage (V)
Streptavidin: MOSHEMT-1
Streptavidin: MOSHEMT-2
Streptavidin: MOSHEMT-3

(d)

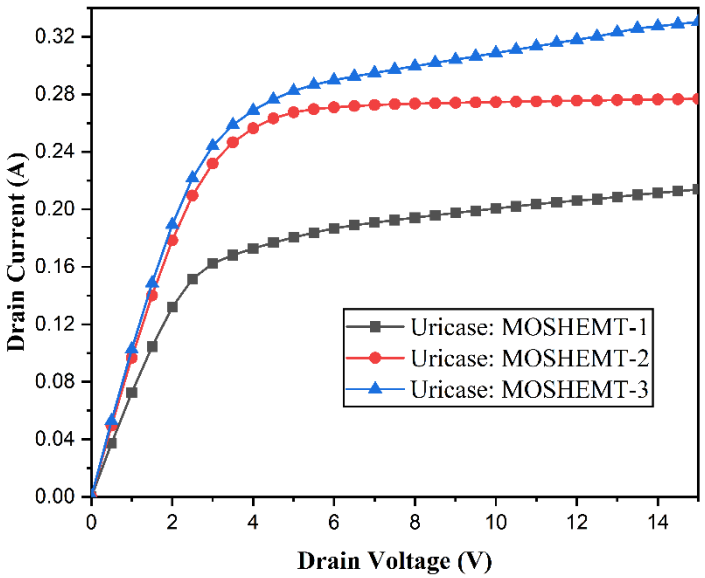

(e)

Fig. 6. I_D-V_D curve for without cavity with V_G=-4 V and different biomolecules using high-K MOSHEMT. MOSHEMT-1: t_{AlGaN}=25 nm, x=0.3, MOSHEMT-2: t_{AlGaN}=18 nm, x=0.3, MOSHEMT-3: t_{AlGaN}=18 nm, x=0.2.

Figure 7(a)-(b) depicts the I_D-V_D and I_D-V_G profiles generated by adding various nano-biomolecules into an embedded nano-cavity with the parameters L_{Cavity}=500 nm, W_{Cavity}=20 nm, t_{AlGaN}=25 nm, and x=0.3. Figure 7(a) demonstrates that the maximum drain current for ChO_X is 0.115 A for SiO_2 MOSHEMTs and 0.164 A for HfO_2 MOSHEMTs at a drain voltage of 15 V, whereas the maximum drain current for Uricase, a biomolecule with a smaller dielectric constant, varies more widely between 0.14 A for SiO_2 MOSHEMTs and 0.214 A for HfO_2 MOSHEMTs at the same drain voltage. Figure 7 (b) shows that the drain current varies by a smaller amount for ChO_X (6.4 mA for HfO_2 MOSHEMT and 4.2 mA for SiO_2 MOSHEMT at V_G=-6 V) than it does for Uricase (24.4 mA for HfO_2 MOSHEMT and 15.4 mA for SiO_2 MOSHEMT at V_G=-6 V).

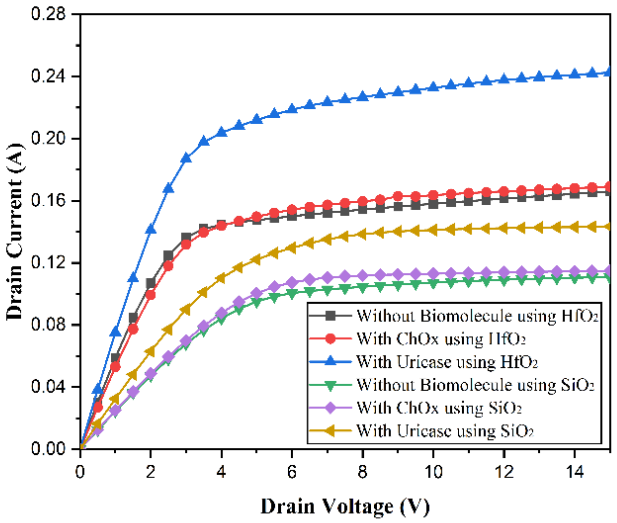

(a)

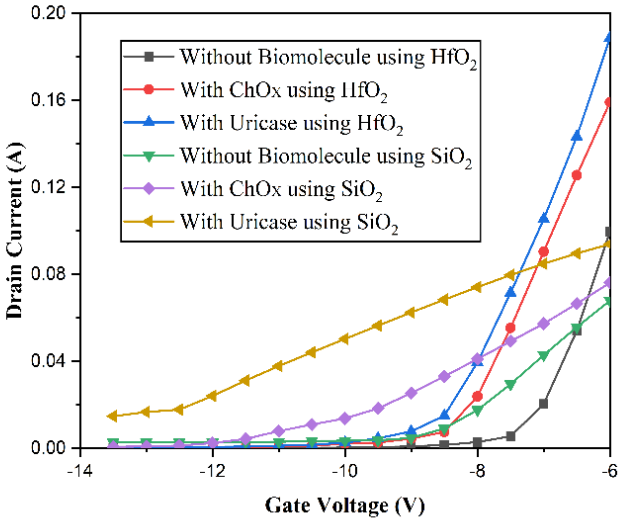

(b)

Fig.7 I_D-V_D and I_D-V_G curves for without cavity with V_D=5 V and for ChOx and Uricase using SiO_2 and HfO_2 MOSHEMT with t_{AlGaN}=25 nm, x=0.3.

Figure 8 (a)–(e) shows the electron concentration variations using high-K MOSHEMT with t_{AlGaN}=18 nm and x=0.2.

Figure 8(a) depicts the negligible change in electron concentration in the absence of biomolecules. When nano-cavity is filled up with biomolecules figure 8 (b)–(e) then more mobile charges will be induced due to capacitive action depending on the permittivity of biomolecule. ChOx with high dielectric constant produces a negligible number of induced charges in the channel, whereas Unicase with low dielectric constant introduces a significant number of induced charges. The electron concentration increases at AlGaN/GaN heterointerface by forming 2DEG. Polarization effect of GaN based HEMT exhibit when it is strained.

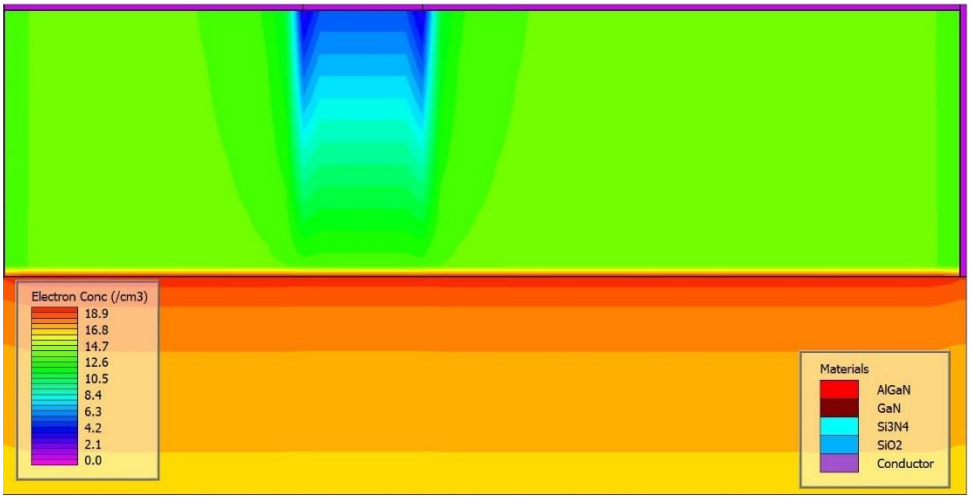
Electron Conc (/cm3)
18.9
16.8
14.7
12.6
10.5
8.4
6.3
4.2
2.1
0.0
Materials
AlGaN
GaN
Si3N4
SiO2
Conductor

(a)

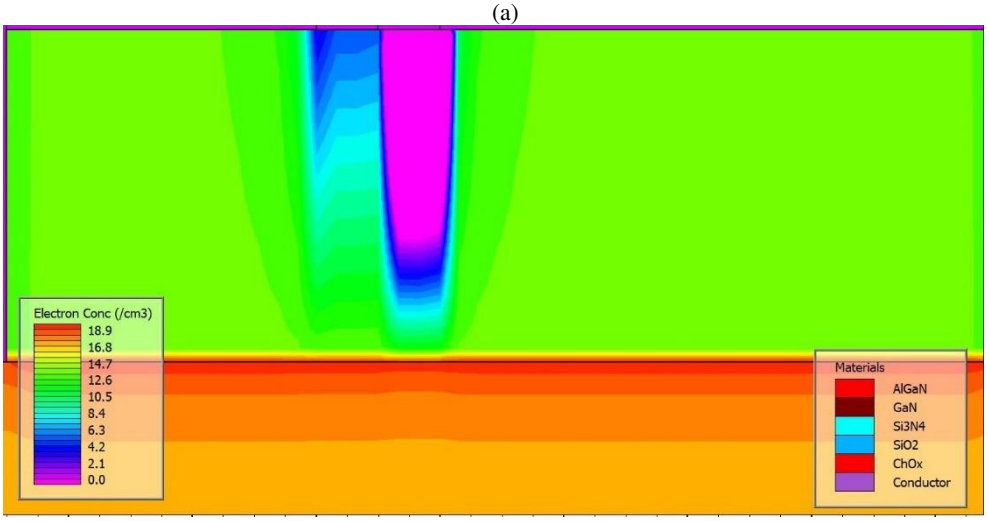
Electron Conc (/cm3)
18.9
16.8
14.7
12.6
10.5
8.4
6.3
4.2
2.1
0.0
Materials
AlGaN
GaN
Si3N4
SiO2
ChOx
Conductor

(b)

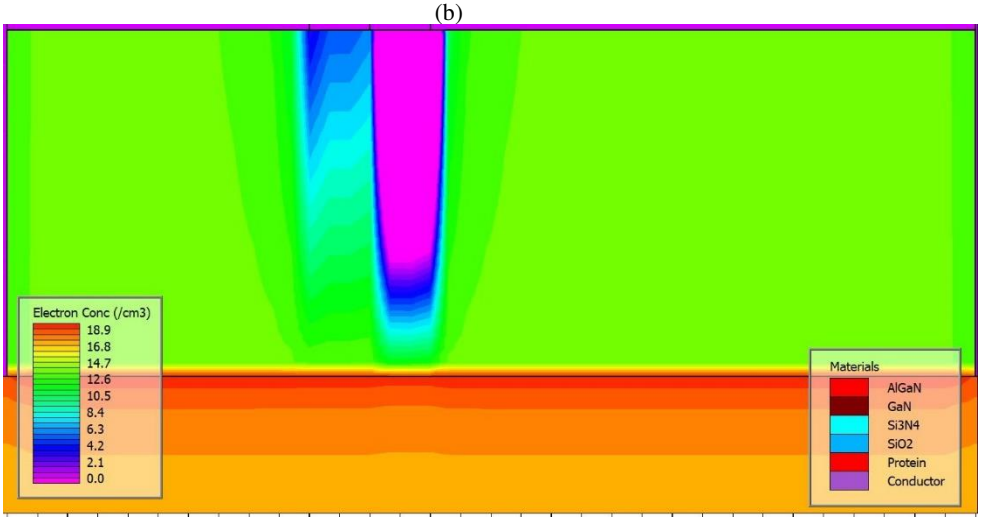
Electron Conc (/cm3)
18.9
16.8
14.7
12.6
10.5
8.4
6.3
4.2
2.1
0.0
Materials
AlGaN
GaN
Si3N4
SiO2
Protein
Conductor

(c)

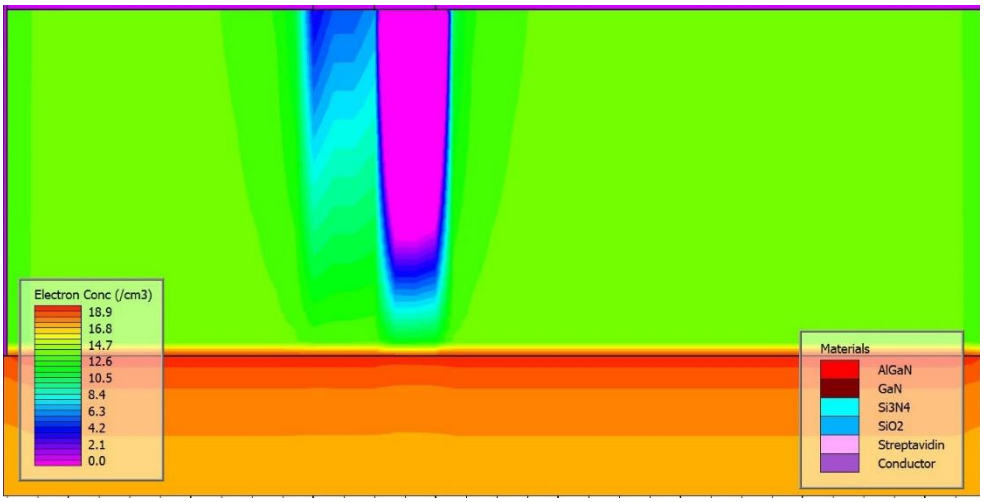

(d)

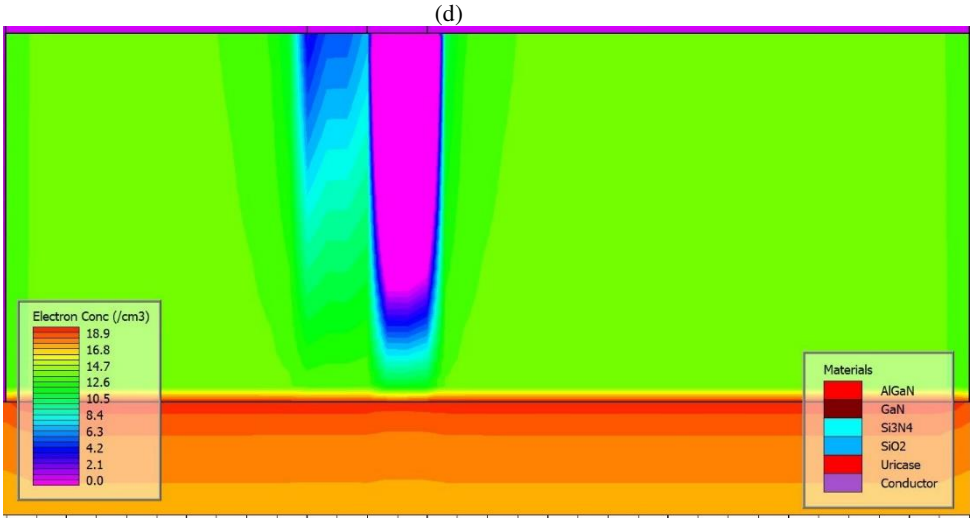

(e)

Fig. 8 Electron density distribution (a)Without biomolecule (b) ChOx (c) Protein (d) Streptavidin (e) Uricase using MOSHEMT based on high-K dielectric with t_{AlGaN}=18 nm and x=0.2.

Due to the existence of more charge carriers, polarization reduces resistivity, allowing for a higher flow of current and a correspondingly larger output of power [5]. The polarization effect might be improved by subjecting the device to mechanical strain. The amount of lattice mismatch between the AlGaN and GaN layers is represented by the pseudomorphic strain.

$$S_{ION} = \frac{I_{ON}(With\ Biomolecule) - I_{ON}(Without\ Biomolecule)}{I_{ON}(Without\ Biomolecule)}$$

I_{ON}(With Biomolecule) and I_{ON}(Without Biomolecule) are is the ON current with biomolecule and without biomolecules respectively. For the measurement of SION, V_G is a constant.

Difference in threshold voltage,

$\Delta V_{th} = V_{th}$ (With Biomolecule) - V_{th} (Without Biomolecule) in V

TABLE I
PERMITTIVITY OF DIFFERENT BIOMOLECULES

Biomolecule	Dielectric Constant
Uricase	1.54
Streptavidin	2.1
Protein	2.5
ChOx	3.3

From this above table 2 (a) MOSHEMT-3 structure using HfO_2 is showing variation in drain current, ΔI_D 45% larger than MOSHEMT-2 while 86% and 90% more in comparison to MOSHEMT-1 and MOSHEMT with SiO_2 [1] respectively. We noticed large change in S_{ION} in MOSHEMT-1 in comparison to other structures in 35% and 56% for MOSHEMT-2 and MOSHEMT-3 respectively. MOSHEMT-1 exhibits better S_{ION} than the latest reported structure by Pal et al. [1].

TABLE II
COMPARATIVE STUDY TABLE OF DIFFERENT ELECTRICAL PARAMETERS

(A)

Electrical parameters	For ChO_X with V_{GS}=-6 V, V_{DS}= 5 V			
	MOSHEMT with SiO_2 [1]	Different Structure of MOSHEMT with HfO_2:		
		MOS HEMT-1	MOS HEMT-2	MOS HEMT-3
ΔI_D(mA)	4.3	6.1	24.0	44.0
ΔV_{th}(V)	0.337243	0.4982	0.5235	0.5648
S_{ION} (600 nm)	0.03163	0.5812	0.376	0.2581
C_{GS}(pF)	0.115	0.05	0.05	0.05

(B)

Electrical parameters	For Protein with V_{GS}=-6 V, V_{DS}= 5 V			
	MOSHEMT with SiO_2 [1]	Different Structure of MOSHEMT with HfO_2:		
		MOS HEMT-1	MOS HEMT-2	MOS HEMT-3
ΔI_D(mA)	11.3	20.1	62.0	55.0
ΔV_{th}(V)	0.733138	0.9448	1.03521	1.0527
S_{ION} (600 nm)	0.06288	0.6396	0.528	0.403
C_{GS}(pF)	0.105	0.038	0.038	0.038

(C)

Electrical parameters	For Streptavidin with V_{GS}=-6 V, V_{DS}= 5 V			
	MOSHEMT with SiO_2 [1]	Different Structure of MOSHEMT with HfO_2:		
		MOS HEMT-1	MOS HEMT-2	MOS HEMT-3
ΔI_D(mA)	13.9	17.1	71.0	79.0
ΔV_{th}(V)	0.879765	1.0498	1.1324	1.2561
S_{ION} (600 nm)	0.07498	0.69112	0.6731	0.6613
C_{GS}(pF)	0.10	0.03	0.03	0.03

(D)

Electrical parameters	For Uricase with V_{GS}=-6 V, V_{DS}= 5 V			
	MOSHEMT with SiO_2 [1]	Different Structure of MOSHEMT with HfO_2:		
		MOS HEMT-1	MOS HEMT-2	MOS HEMT-3
ΔI_D(mA)	15.9	39.1	87.0	98.0
ΔV_{th}(V)	1.055718	1.3938	1.4128	1.4362
S_{ION} (600 nm)	0.08535	0.73997	0.7489	0.7944
C_{GS}(pF)	0.095	0.027	0.027	0.027

From this above table 2 (d) MOSHEMT-3 is showing variation in drain current, ΔI_D 11% larger than MOSHEMT-2 while 60% and 84% more in comparison to MOSHEMT-1 and MOSHEMT with SiO_2 [1] respectively. We observed a significant change in S_{ION} in MOSHEMT-3 in comparison to other structures in 5% and 7% for MOSHEMT-2 and MOSHEMT-1 respectively. Moreover MOSHEMT-3 is shown better S_{ION} than the latest reported structure by Pal et al. [1].

Figure 9 depicts capacitance from gate to source (C_{GS}) as a function of gate voltage (V_G). C_{GS} is demonstrated to peak at approximately 0.95 pF close to -5.5 V for no cavity, decrease with increasing gate voltage, and reach a minimum of 0.86 pF close to 1 V. For gate voltages ranging from -4.5 V to 1 V, the capacitance of each biomolecule is found to be unaffected. In Pt Schottky contacts, the capacitance between the gate and the source changes dramatically.

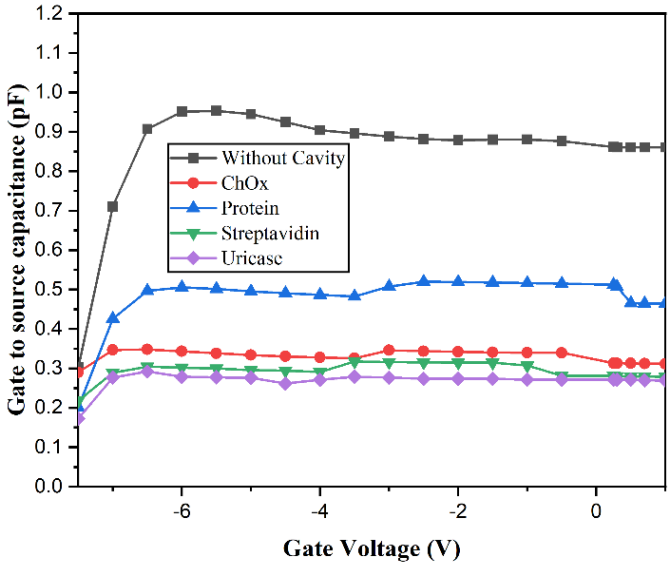

Fig. 9 C_{GS}- V_G curves for without cavity and different biomolecules using high-K MOSHEMT.

As shown in Figure 10, the drain-on sensitivity (S_{ION}) varies between biomolecules. Increasing the nano-cavity length varies from 400 nm to 600 nm which enhances the quantity of biomolecules that interact with the AlGaN layer, resulting in a maximal variation in sensitivity of 0.7944 for Uricase. Changes in charge density in response to a drain current are caused by biomolecular interaction. As shown in Figure 10, biomolecules with a reduced dielectric constant are more sensitive.

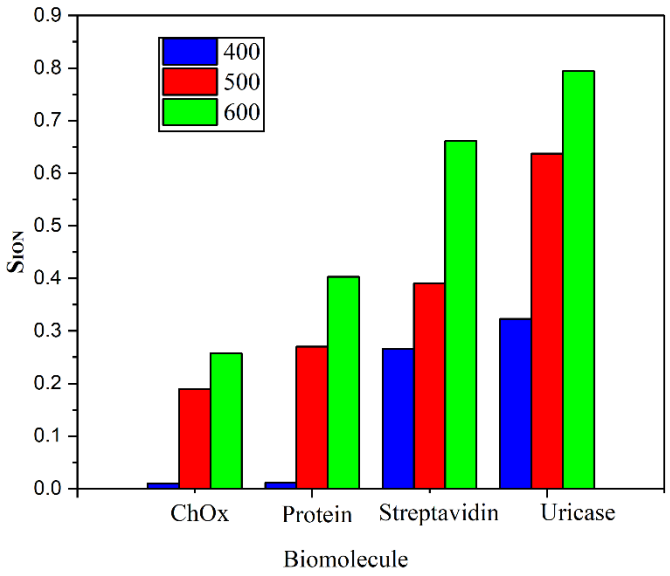

Fig. 10 Variation of S_{ION} for different biomolecules.

Figure 11 demonstrates that, in comparison to the structure described by Pal et al. [1], the proposed structure is approximately nine times more sensitive.

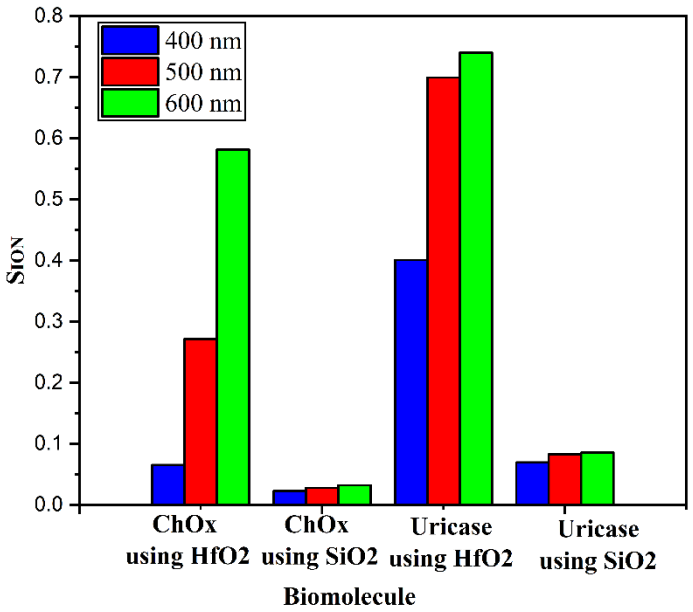

Fig. 11 Drain-on-sensitivity (SION) for ChO_X and Unicase biomolecules for t_{AlGaN}=25 nm, x=0.3, using SiO_2 and HfO_2 respectively.

5. Proposed Fabrication Method

Superlattice nano-scale AlGaN/GaN high-k MOSHEMTs could be fabricated using a multi-step process comprising of several deposition and patterning processes. following is a summary of a method given for creating such a device:

Substrate Preparation: could be started with a suitable substrate with a high-quality surface, such as Sapphire. Standard cleaning step would be adopted to get rid of any impurities.

Buffer Layer Growth: To solve the problem of lattice mismatch between the Sapphire substrate and succeeding layers, a buffer layer should be deposited on the substrate. This is often accomplished via the use of MBE or MOCVD. AlN is often used for the buffer layer because it provides a high-quality, uniform base upon which succeeding layers may be built.

AlGaN/GaN Superlattice Growth: Growth of a superlattice structure of AlGaN and GaN layers would be done using MOCVD or MBE route. Al mole fraction will be adjusted suitably for the optimized growth of AlGaN/GaN layer for regulation of the electrical characteristics. Device performance may be adjusted by changing the thickness of the superlattice layer.

High-K Dielectric Deposition: On top of the AlGaN/GaN superlattice, high-k dielectric layer such as Hafnium oxide (HfO_2) would be deposited. To effectively regulate the transistor channel, the high-k dielectric is used as a gate insulator.

Gate Electrode Formation: To create the gate electrode, a layer of metal such as platinum (Pt) or nickel gold (Ni/Au) would be deposited on top of the high-k dielectric. The size and form of the gate electrode may be customized using photolithography and etching.

Ohmic Contact Formation: An aluminium layer of appropriate thickness may be incorporated to form the ohmic contacts for the source and drain regions. The photolithography and mesa- etching would be done for formation of the source and drain contacts on the metal layer.

Junction Passivation and Interconnects: A passivation layer, such as silicon nitride (Si_3N_4) would be introduced to protect and enhance the stability of the device. Create contact windows through the passivation layer for wire bonding and other interconnections using additional photolithography and etching steps.

Backside Processing: Backside processing such as thinning the substrate or adding would be done for specific device requirements for backside contact layer formation.
Testing and Characterization: The electrical testing and characterization of the fabricated devices would be performed in order to evaluate the performance parameters, including current-voltage characteristics, gate-source capacitance characteristics, and sensitivity. It is essential to observe that the proposed fabrication method may vary based on specific research or industry needs. To accomplish the desired device performance, the microelectronics fabrication stages, including material selection, growth conditions, and process parameters, must be optimized.

6 Conclusions

The sensitivity of biosensors based on High-K MOSHEMTs has been enhanced in comparison to biosensors based on SiO_2 MOSHEMTs. Increased capacitance due to high-K material may be provided by the surface biomolecules. Capacitance and surface potential are found to be related to sensitivity. The suggested structure incorporates high-K material for label-free biosensing, increasing its sensitivity in comparison to biosensors based on SiO_2 MOSHEMTs. Changes have been observed in both V_{th} and C_{GS}. The reliability of the model is confirmed by the results of the experiments. Our simulated results are suitable for the device structural optimization with high-K dielectric for efficient label free detection of biomolecules.

Acknowledgement

The authors wish to convey their appreciation to Adamas University and the National Institute of Technology (NIT), Mizoram for offering them with the essential resources to conduct their research. Dr. M. Mukherjee is deeply grateful to DRDO, India for supporting the work on the development of GaN/AlGaN epilayers.

Declarations

Ethical Approval

No ethical approval is required.

Funding

The research is partially supported by DRDO, Ministry of Defence, throgth extramural research project.

Availability of data and materials

No external dataset is used.

References

1. Praveen Pal, Yogesh Pratap, Mridula Gupta and Sneha Kabra, "Modeling and Simulation of AlGaN/GaN MOS-HEMT for biosensor applications," IEEE Sensors Journal, vol. 19, no. 12, pp. 587 - 593, Oct.2018.
2. Shaveta, H. M. Maali Ahmed and Rishu Chaujar " Rapid detection of biomolecules in a dielectric modulated GaN MOSHEMT," Springer, Aug.2020.
3. G. Dechun, Q. Kankan, C. Junfeng, L. Xiaobin and Y. Chao, "A simulation about the influence of the gate-source-drain distance on the AlGaN/GaN HEMT performance at Ka-band," In Microwave Workshop Series on Millimeter Wave Wireless Technology and Applications (IMWS), IEEE MTT-S International , pp. 1-4, Sep.2012.
4. S. Russo and A. Di Carlo, "Influence of the source–gate distance on the AlGaN/GaN HEMT performance," IEEE Transactions on Electron Devices, Vol.54, no.5, pp.1071-1075, May.2007.
5. W. D. Hu, X. S. Chen, Z. J. Quan, X. M. Zhang, Y. Huang, C. S. Xia, W. Lu, and P. D. Ye, " Simulation and optimization of GaN-based metal-oxide-semiconductor high-electronmobility-transistor using field-dependent drift velocity model," Journal of Applied Physics, 2007
6. R. Dingle, H. L. Stormer, A. C. Gossard, and W. Wiegmann, "Electron Mobilities in Modulation-Doped Semiconductor Heterojunction Superlattices," Appl. Phys. Lett., 33, 665 (1978).

7. K. H. Chen, B. S. Kang, H. T. Wang, T. P. Lele, F. Ren, Y. L. Wang, C. Y. Chang, S. J. Pearton, D. M. Dennis, J.W. Johnson, P. Rajagopal, J. C. Roberts, E. L. Piner, and K. J. Linthicum, "c-erbB-2 sensing using Al Ga N ⁄ Ga N high electron mobility transistors for breast cancer detection," Journal of Applied Physics, 2008.
8. J M. Choi, J. W. Han, S. J. Choi, and Y. K. Choi, "Analytical modeling of a nanogap-embedded FET for application as a biosensor," IEEE Transactions on Electron Devices, vol. 57, no. 12, pp. 3477-3484, Dec.2010.
9. D. Kim, Y. T. Jeong, H. J. Park, J. K. Shin, P. Choi, J. H. Lee, and G. Lim, "An FET-type charge sensor for highly sensitive detection of DNA sequence," Biosensors and Bioelectronics, vol. 20, no. 1, pp. 69-74, Jul.2004.
10. C. Kim, C. Jung, K. B. Lee, H. G. Park and Y. K. Choi, "Label-free DNA detection with a nanogap embedded complementary metal oxide semiconductor," Nanotechnology, vol. 22, no. 13, pp. 135502, Feb.2011.
11. B. Gu, T. J. Park, J. H. Ahn, X. J. Huang, S. Y. Lee, and Y. K. Choi, "Nanogap field-effect transistor biosensors for electrical detection of avian influenza," small, vol. 5, no. 21, pp. 2407-2412, Nov.2009.
12. I. Maesoon, J. H. Ahn, J. W. Han, T. J. Park, S. Y. Lee, and Y. K. Choi, "Development of a point-of-care testing platform with a nanogap-embedded separated double-gate field effect transistor array and its readout system for detection of avian influenza," IEEE Sensors journal, vol. 11, no. 2, pp. 351-360, Feb.2011.
13. S. Deblina, H. Gossner, W. Hansch, and K. Banerjee, "Impact-ionization field-effect-transistor based biosensors for ultra-sensitive detection of biomolecules," Applied Physics Letters, vol. 102, no. 20, pp. 2031101-2031105, May.2013.
14. S. Deblina, and K. Banerjee, "Proposal for tunnel-field- effect-transistor as ultra-sensitive and label-free biosensors," Applied Physics Letters, vol. 100, no. 14, pp. 1431081-1431084, Apr.2012.
15. M. Kenzo, T. Katsura, K. Kerman, Y. Takamura, K. Matsumoto, and E. Tamiya, "Label-free protein biosensor based on aptamer-modified carbon nanotube field-effect transistors," Analytical Chemistry, vol. 79, no. 2, pp. 782-787, Jan.2007.
16. N. Kannan, and M. J. Kumar, "Charge-modulated underlap I-MOS transistor as a label-free biosensor: A simulation study," IEEE Transactions on Electron Devices, vol. 62, no. 8, pp. 2645-2651, Aug.2015.
17. G. Seo, G. Lee, J.-O. Lee, B.T. Kim, E.C. Park, S.I. Kim, "Rapid detection of COVID-19 causative virus (SARS-CoV-2) in human nasopharyngeal swab specimens using field-effect transistor based biosensor". Am. Chem. Soc. 14(4), 5135–5142, 2020.
18. Y. Pratap, M. Kumar, S. Kabra, S. Haldar, R.S. Gupta, M.Gupta, "Analytical modeling of gate-all-around junctionless transistor based biosensors for detection of neutral biomolecule species." J. Comput. Electron. 17, 288–296, 2018.
19. Chang Liu, Eng Fong Chor, and Leng Seow Tan, "Investigations of HfO2/AlGaN⁄GaN metal-oxide-semiconductor high electron mobility transistors," Applied Physics Letters, vol. 88, pp. 173504-1- 173504-3, 2006.
20. Y. Y. Zheng , Y. Hao, Q. Feng, J. C. Zhang, X. H. Ma, and J. Y. Ni, "Study of GaN MOS-HEMT using ultrathin Al2O3 dielectric grown by atomic layer deposition," Science in China Series E: Technological Sciences, vol. 52, no. 9, pp. 2762-2766, Sep.2009.
21. O. Ambacher, J. Smart, J. R. Shealy, N. G. Weimann, K. Chu, M. Murphy, W. J. Schaff, L. F. Eastman, R. Dimitrov, L. Wittemer and M. Sturtzmann, "Two dimensional electron gases induced by spontaneous and piezoelectric polarization in undoped and doped AlGaN/GaN heterostructures," Journal of applied physics, vol. 87, no. 1, pp. 334-344, Jan.2000.
22. Y. F. Mulugeta, S. Khandelwal, T. A. Fjeldly, and B. Iñiguez, "Compact charge-based physical models for current and capacitances in AlGaN/GaN HEMTs," IEEE Transactions on Electron Devices, vol. 60, no. 11, pp. 3746-3752, Nov.2013.
23. S. Kola, J. M. Golio, and G. N. Maracas, "An analytical expression for Fermi level versus carrier concentration for HEMT modeling," IEEE Electron Device Lett., vol. 9, no. 3, pp. 136–138, Mar. 1988.
24. D. Delegebeaudeuf and N. T. Linh, "Metal-(n)AlGaAs-GaAs two dimensional electron gas FET," IEEE Electron Device Lett., vol. 29, no. 6, pp. 955–960, Jun. 1982.